ACS APPLIED MATERIALS & INTERFACES

www.acsami.org Research Article

Ductile Shape-Memory Polymer Composite with Enhanced Shape Recovery Ability

Kaiyuan Peng,[†] Yao Zhao,[†] Shima Shahab, and Reza Mirzaeifar*

Cite This: https://dx.doi.org/10.1021/acsami.0c18413 Read Online

ACCESS | Metrics & More | Article Recommendations | Supporting Information

ABSTRACT: In recent years, shape-memory polymers (SMPs) have received extensive attention to be used as actuators in a broad range of applications such as medical and robotic devices. Their ability to recover large deformations and their capability to be stimulated remotely have made SMPs a superior choice among different smart materials in various applications. In this study, a ductile SMP composite with enhanced shape recovery ability is synthesized and characterized. This SMP composite is made by a mixture of acrylate-based crosslinkers and monomers, as well as polystyrene (PS) with UV curing. The composite can achieve almost 100% shape recovery in 2 s by hot water or hot air. This shape recovery speed is much faster than typical acrylate-based SMPs. In addition, the composite shows excellent ductility and viscoelasticity with reduced hardness. Molecular dynamics (MD) simulations are performed for understanding the curing mechanism of this composite. With the combination of the experimental and computational works, this study paves the way in front of designing and optimizing the future SMP devices.

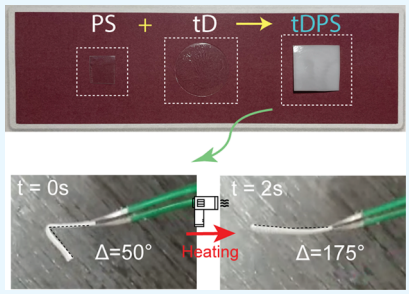

KEYWORDS: *shape memory polymer composite, tertbutyl acrylate (tBA), polystyrene (PS), mechanical properties, molecular dynamics (MD)*

1. INTRODUCTION

Shape memory polymers (SMPs) are a class of smart materials that can store one or more intermediate shapes and recover to their permanent shape when subjected to an external stimulus.[1−4] The ability of being responsive to multiple stimuli[5] enables SMPs a superior choice for applications in soft actuator and soft robotics.[6,7] For certain types of SMPs,[8] being biodegradable and biocompatible also make them potential candidates in biosensing[9,10] and controlled drug delivery fields.[11−14] SMPs can be usually categorized into several types, namely, chemo-/thermoresponsive,[15−19] and photoresponsive SMPs.[20] When the temperature rises, the thermoresponsive SMPs absorb heat to accomplish shape recovery due to the inner phase transition or component softening/transition.[18] Compared to traditional shape-memory materials, such as shape-memory alloys[21,22] and shape-memory ceramics,[23] SMPs are flexible, inexpensive, lightweight, and consequently applicable in a broad range of devices. Because of these advantages of SMPs, the study of their properties has received extended attention in the past several years.

Among multiple types of SMPs, acrylate-based AB copolymer networks, obtained from the copolymerization of monomers and crosslinkers, have remarkable advantages such as the biocompatibility,[24,25] relative ease of preparation,[26] and three-dimensional/four-dimensional (3D/4D) printability.[27−29] For instance, Yu et al. demonstrated a photopolymer printable *tert*butyl acrylate (*t*BA)-*co*-di(ethylene glycol) dimethacrylate (DEGMA) network.[30] Using the stereolithography apparatus (SLA) technology, thermoresponsive acrylate-based SMPs with complex geometry can be fabricated. Hongzhi and co-workers also presented a four-dimensional printing method to fabricate acrylate-based SMPs.[31] Antony et al. synthesized a type of SMPs using *t*BA and poly(ethylene glycol) dimethacrylate (PEGDMA). The synthesized SMP sample can recover from the deformed shape (a deformed M-shape filament) to the permanent shape (a straight filament) in 45 s after being completely immersed in 55 °C hot water. By adding diurethane dimethacrylate (DUDMA) to the existing *t*BA-PEGDMA SMP matrix, the shape recovery rate of this SMP network become around 20 s for full recovery.[32]

Despite many works reported on fabricating efficient SMPs, experiments have shown that fulfilling a ∼100% shape recovery within a few seconds (<10 s) is still challenging. If SMPs have a large recovery percentage and fast response, it will make them a good candidate for being used as remote actuators. One example is the high-intensity focused ultrasound (HIFU) induced *in vivo* drug delivery system because HIFU can remotely and noninvasively actuate SMPs. However, the actuation is usually slow, and the recovery percentage is low, which emerges the

Received: October 14, 2020
Accepted: December 8, 2020

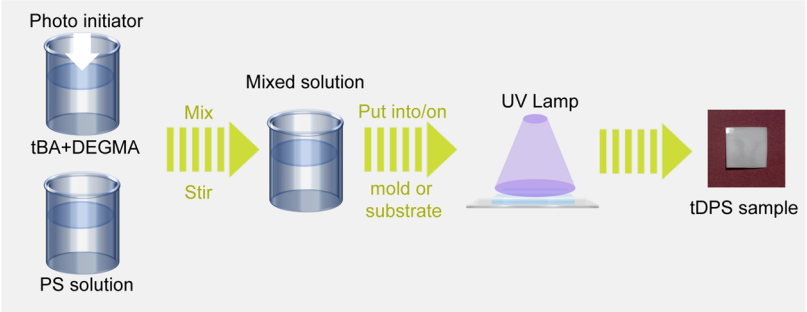

Figure 1. Schematic showing processing steps to prepare a *t*DPS composite.

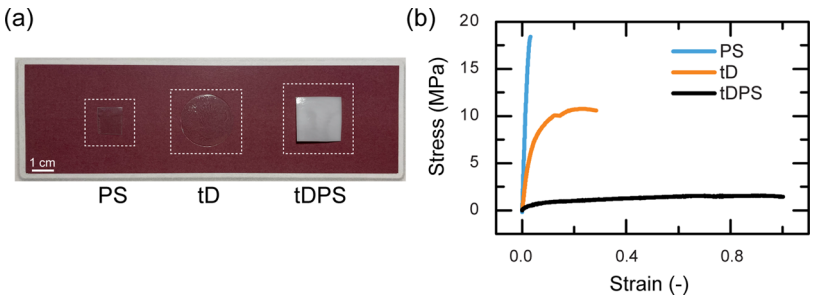

Figure 2. Digital image (a) and stress−strain curves (b) of PS, *t*D, and *t*DPS samples.

need for new classes of SMPs with large recovery percentage and a fast response. We have recently investigated the influence of the chemical composition of SMPs on HIFU-induced shape recovery.[11,33−35] In these works, *t*BA and DEGMA were used as monomer and crosslinker to synthesize SMPs. It was shown that the chemical composition (the ratio of monomer to crosslinker) has a significant effect on the final shape recovery ratio of SMPs (Need to note that selecting a proper programming temperature can also help optimize the shape recovery performance even without modifying its composite,[36,37] but we choose to tune the chemical composite in this work). Tuning the composition ratio could help achieve a higher shape recovery ratio after a 20 s continuously ultrasonic exposure. However, the maximum recovery ratio was around 20%. In our recent study, it was found that the HIFU-induced thermal effect for polymers is closely associated with the viscoelasticity of materials.[38] The viscous damping caused by the HIFU results in an obvious heating difference. The computational works indicated that more heat is generated in viscoelastic amorphous polymers when they are subject to HIFU compared to crystalline polymers.

Therefore, to design more efficient HIFU-induced SMP devices, the targeted properties of SMPs fall into two aspects. On the one hand, the actuation of SMPs should be efficient, which means sufficient heat can be accumulated at relatively low acoustic power exposure. On the other hand, SMPs should have adequate recoverability, which is closely associated with the elastic part (the crosslinking in the thermoset material). It refers that SMPs can achieve fast full recovery, such as a 95% or more recovery ratio within 10 s, when subject to traditional heat sources (like hot water or air). In this study, an acrylate-based polymeric composite with a superior shape-memory ability is synthesized. This composite can achieve almost 100% shape recovery ratio within 2 s under hot air/water. From the dynamic mechanical analysis (DMA) test, it is observed this composite also have relatively large viscoelasticity, which may lead to a good thermic response triggered by HIFU. Nanoindentation tests are also conducted to further explore the related mechanical properties of this composite. Additionally, molecular dynamics (MD) simulations are also performed to study the reasons behind these properties at the atomistic scale by investigating the crosslinking mechanism for the curing process of this composite.

2. MATERIALS AND METHODS

tert-Butyl acrylate (*t*BA), di(ethylene glycol) dimethacrylate (DEGMA), polystyrene (PS) pellets with typical molecular weights of M_n = 35 000, toluene (anhydrous, 99.8%), and the photoinitiator 2,2-dimethoxy-2-phenyl-acetophenone were purchased from Sigma-Aldrich and used as received condition without further alternation. Molds are ordered from Allied High Tech Products, Inc. In a typical experiment, *t*BA (monomer) and DEGMA (crosslinker) were first mixed at a weight ratio of 85:15, followed by 1 wt % photoinitiator added into the solution. The solution was then fully stirred for 20 min. In addition, 1.5 g of PS pellets were added into 8.5 g of toluene. The solution was stirred at 50 °C for 2 h to make PS pellets fully dissolved. The prepared *t*BA−DEGMA solution and PS solution were mixed at a weight ratio of 85:15 (2.55 g of *t*BA−DEGMA solution and 0.45 g of PS solution in this case) and stirred for another 20 min. Afterwards, the resultant mixture was cured in a Teflon open mold (without cap) with 365 nm UV light exposure for 15 min. The prepared SMP composites, namely, *t*DPS, were postcured inside the fume hood for 24 h. The *t*DPS sample is cut into 10 mm × 2 mm × 1 mm strip for mechanical tests and 25 mm × 3 mm × 1 mm for the shape recovery test. The entire synthesis procedures are shown in Figure 1.

To provide a comparison between *t*BA−DEGMA SMP (we will call it *t*D in all following sections for convenience), PS and the *t*DPS samples, pristine *t*D and PS samples were obtained by UV curing and the drop casting method separately. A detailed synthesis method for *t*Ds is in our previous paper.[11] For PS samples, 1.5 g of PS pellets were dissolved into 8.5 g of toluene. The well-mixed solution was then dropped on a 25 mm × 25 mm mica substrate (Highest Grade V1, Ted pella). A pristine PS film can be easily peeled off from the mica substrate after 24 h solvent evaporation in fume hood.

The uniaxial tensile tests and dynamic mechanical analysis (DMA) were measured by a universal testing system (MTS Tytron 250). The tensile tests were performed with a strain rate of 0.0067 s^{-1}

https://dx.doi.org/10.1021/acsami.0c18413
ACS Appl. Mater. Interfaces XXXX, XXX, XXX−XXX

(displacement control). In addition, dynamic mechanical thermal analysis is also done by a TA-Q800 DMA tester (TA Instruments) to measure the storage modulus, loss modulus, and tan delta for the samples. The oscillation frequency is 1 Hz, and the temperature is increased at a rate of 2 °C/min. Differential scanning calorimetry (DSC) measurements were performed on a TA-Q200 DSC tester (TA Instruments). The samples in the aluminum pans were analyzed under nitrogen condition at a heating rate of 5 °C/min. Testing cycles were run from 30 to 120 °C. In addition, the mechanical tests in the out-of-plane direction of the samples were conducted by a nanoindenter (Hysitron TI950, Eden Prairie, MN). The peak load 500 μN was held for 1 s with a loading and unloading rate of 50 μN/s. The depth at the peak loading is small enough to maintain a quasistatic state.

Molecular dynamics simulations were performed to investigate the crosslinking mechanism during the curing process of *t*DPS and *t*D. All simulations were implemented by the molecular dynamics simulator LAMMPS.[39] Two simulation systems, one contains *t*BA, DEGMA and PS monomers/chains, and another only contains *t*BA and DEGMA, were created using the open-source package Moltemplate[40,41] and Packmol.[42,43] The postprocessing is processed by the software Ovito.[44] Each simulation takes around 4 h on 48 CPUs.

3. RESULTS AND DISCUSSION

Samples made of PS, *t*D, and *t*DPS prepared by the methods described in the previous section are shown in Figure 2a. From DSC and DMA measurements (Figures S1−S5), the glass transition temperature of PS is 95 °C and the transition ranges of *t*D and *t*DPS samples are from 60 to 80 °C. Notably, although PS and *t*D are transparent polymers, *t*DPS, as a combined composite of PS and *t*D, is a type of white material with relatively low transparency. These samples are then cut into strips to perform a uniaxial tensile test. It can be found that PS and *t*D are brittle while *t*DPS is a ductile material. As shown in Figure 2b, the stress of PS increases dramatically at the initial regime of strain and breaks at a strain level of ∼0.03. A pronounced increase also presents at the early stage of the stress curve of *t*D. The *t*D yields at a stress of 10.5 MPa, then breaks at ∼0.3 strain. In contrast, *t*DPS shows a significantly different stress−strain response. The material stiffness decreases prominent with an extended ductility. The young's modulus of PS, *t*D, and *t*DPS are 597.24, 270.12, and 39.55 MPa, respectively. The maximum stress of *t*DPS during the tensile test is ∼1.5 MPa, and the sample can be elongated to a strain of 1 without breaking. The possible reasons for this mechanical response variation will be investigated later by MD simulation.

The programming and shape recovery process of the *t*DPS sheet are shown in Figure 3. The initially flat (permanent shape) *t*DPS sample is deformed to an angle of 5°. The deformed shape (intermediate shape) is programmed for 10 s. After the load releases, the bended sample will return to an angle of 50° automatically because of the elastic component in the material.[36] Subsequently, a regular hair dryer is used to apply hot air to the sample. As shown in Figure 3 and the video (Movie S1, Supporting Information), it is observed that the filament will return to its initial shape (Δ = 175°) within 2 s after heating by the hair dryer. In another scenario (Movie S2, Supporting Information), the deformed composite is immersed into hot water (temperature ∼65 °C); the sample also shows a very fast recovery to its original shape (flat shape, Δ = 175°). Notably, although bending has some limitations to characterize shape-memory effect, such as the strain in the bended area is not uniform.[45] However, bending is one of the most common used and straightforward ways to evaluate the performance of shape-memory effects quantitively. In this study, we still use bending and tracking the change of bended angle to characterize the shape recovery ability of the samples.

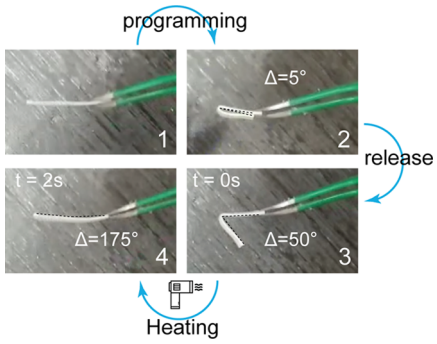

Figure 3. Illustrations of the programming and recovery of the *t*DPS sheet sample. See text and the videos in the Supporting Information for details.

The synthesized *t*DPS is able to achieve good temporal and spatial effects. From Figure 3, the *t*DPS sample has almost 100% shape recovery, which is 5 times more than the maximum shape recovery of *t*D (∼20%) shown in our previous work.[11] A very quick response (recovery in 2 s) is also observed when direct heat is applied. The better recovery degree can be due to the improved thermal processability.[2] These results show that the *t*DPS has a remarkably better recovery ability compared to *t*D.

The tensile stress hysteresis loop of the *t*DPS sample is shown in Figure 4a. The test was performed with loading/unloading rate is 0.0067 s^{-1} without any peak load holdings. The large areas in the hysteresis illustrate the high viscoelasticity of the composite, given the fact that the loading and unloading locus will overlap for ideal elastic material.[46,47] To further explore the mechanical properties of *t*DPS, the DMA test is performed. A 10% prestrain is first applied on the sample, and then the sample is subjected to cyclic loading and unloading with constant strain rates. The frequency is 1 Hz, and the amplitude is 10% strain. In Figure 4b, there is a 56.14° phase lag between the stress−strain curves on average, which again indicates the high viscoelasticity of the *t*DPS sample.

It is worth noting that the viscoelasticity makes *t*DPS having a great potential for being actuated with HIFU. The vibration-induced damping loss and viscous internal friction inside *t*DPS may result in an obvious heating effect, even when the power level of the trigger (HIFU) is relatively low. In this way, the "onset" shape recovery temperature can be reached when subject to lower-level acoustic power, which helps to avoid the unpredictable damage inside the polymer and easier actuation for soft actuator applications.

As shown in Figure 5a, the reduced Young's Modulus of the PS, *t*D, and *t*DPS samples are 4.46, 3.72, and 0.02 GPa separately. Figure 5b compares the hardness of PS, *t*D, and *t*DPS samples by nanoindentation. Figure 5c shows typical loading−unloading curves for the samples during the nanoindentation test. The *t*DPS sample shows a much larger indentation depth (displacement in the indenting direction) at the peak loading because hardness depends on stiffness and strength. Grouping Figure 5a−c, these results correspond well with tensile test results in Figure 2b.

A question that needs to be answered here is why *t*D and *t*DPS show totally different mechanical properties. As mentioned, *t*D is synthesized from the mixture of DEGMA and *t*BA, while *t*DPS is cured from the mixed solution of DEGMA, *t*BA, and PS. We hypothesize that PS plays an important role during the UV

https://dx.doi.org/10.1021/acsami.0c18413
ACS Appl. Mater. Interfaces XXXX, XXX, XXX−XXX

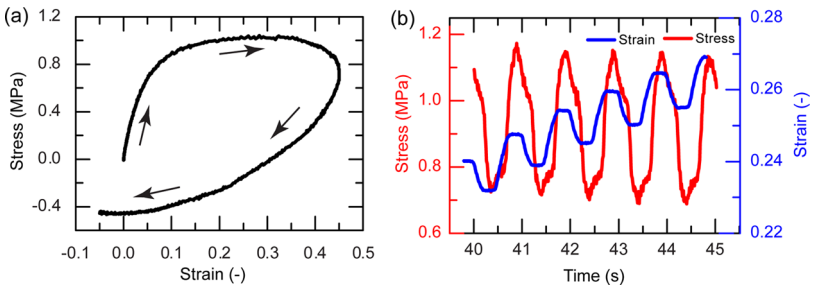

Figure 4. (a) Stress hysteresis loop of *t*DPS composites and (b) corresponding phase lags between stress and strain by the DMA test.

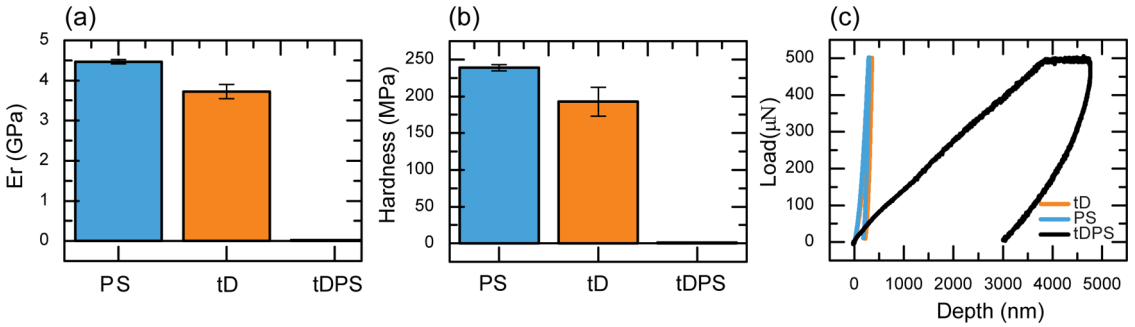

Figure 5. Reduced Young's Modulus (a), the hardness (b), and the load−displacement profiles (c) of the samples by nanoindentation tests.

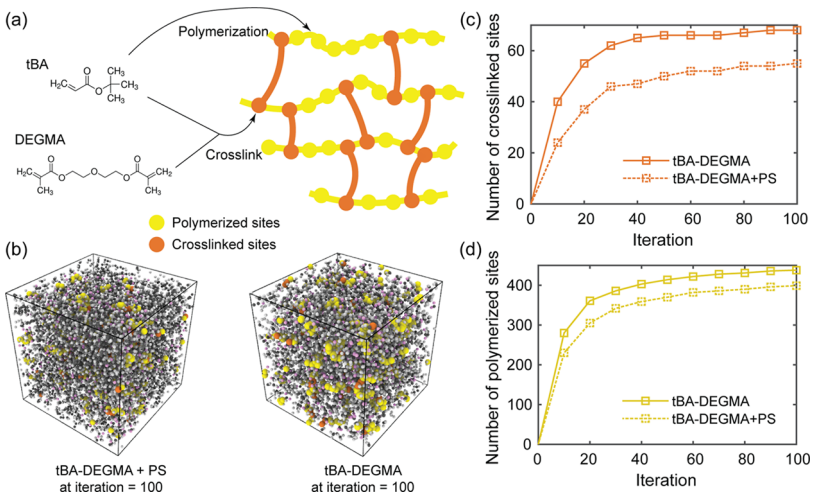

Figure 6. (a) Schematics of polymerization and crosslinks of *t*BA (monomer) and DEGMA (crosslinker) during the polymer UV curing process. (b) Representation of *t*DPS (*t*BA−DEGMA + PS) and *t*D (*t*BA−DEGMA) systems in the simulation box. Periodic boundary conditions are applied in *x*, *y*, and *z* directions. (c) and (d) show the evolution of crosslinked sites and polymerization sites for these two systems for the entire curing process (iterations from 0 to 100).

curing procedure and investigate the potential mechanism with MD simulations. Figure 6a displays the schematic of the UV curing process.[30,31] The monomers of *t*BA would polymerize together into long chains and finally form the crosslinked network with the crosslinker DEGMA. Two MD simulation boxes are created with periodic boundary conditions in *x*, *y*, and *z* directions. Each simulation box contains 288 *t*BA monomers and 27 DEGMA crosslinkers (the mass ratio of *t*BA and DEGMA molecules is 85:15), separately. One of the boxes also has 27 short PS chains (chain length $N = 8$) inside. There are one active polymerization site on every *t*BA molecule and two active crosslinking sites on DEGMA. A distance-based bond creation criterion for the polymerization and crosslinking is used. Specifically, a new bond will form when the distance of two active sites is shorter than 4.5 Å. Note that the new bond can only form between different molecules. To avoid sudden energy jump, which may result in nonequilibrium, the system will then equilibrate by NVT (constant substance amount N, constant volume V, and constant temperature T) and NPT (constant substance amount N, constant pressure P, and constant temperature T) ensembles, as well as the energy minimization process. After the systems reach equilibrium again, a new iteration can be started. CVFF potential force file[48] is used in all MD simulations. The motion equations in the simulations are integrated by velocity−Verlet algorithm with a timestep of 1 fs. The temperature is held at 330 K by Nosé−Hoover thermostat with a damping constant of 0.1 ps.

The schematic representation of the polymeric system after polymerization and crosslinking (iteration = 100) is illustrated in Figure 6b. The polymerized and crosslinked sites are

https://dx.doi.org/10.1021/acsami.0c18413
ACS Appl. Mater. Interfaces XXXX, XXX, XXX−XXX

highlighted in yellow and orange, respectively. Figure 6c,d shows the evolution of the number of crosslinked and polymerized sites. Grouping Figure 6b−d, it is found that the added PS can hinder the polymerization and crosslinking processes by 9.77 and 23.64%, separately, which prevent the mixture form a tightly crosslinked network during the curing process. Notably, the PS chain length in MD simulation is much shorter than in real experiments; so the quantitative values (9.77 and 23.64%) here only provides a lower boundary threshold. The decreased polymerization and crosslinking rates will result in shorter molecular chains and looser networks, which enables larger local molecular mobilities. Hence, the *t*DPS has a lower stiffness and hardness compared to the well-crosslinked *t*D. Additionally, short chains and the loose network can also yield to more liquidus behaviors, in other words, higher viscoelasticity. On the other hand, it is worth noting that pristine PS is a brittle material with relatively high stiffness. This is because lots of entanglements are inside the pure PS system. For *t*DPS in this case, PS chains are much less entangled due to the obstructs of *t*BA and DEGMA, which finally makes *t*DPS a ductile material.

4. CONCLUSIONS

In this study, a novel shape-memory composite *t*DPS is synthesized and systematically studied by experiments and molecular dynamics simulations. The composite exhibits enhanced shape recovery ability, which can reach almost 100% recovery ratio in 2 s triggered by hot air or water. From corresponding mechanical tests, the composite shows reduced hardness and relatively high viscoelasticity. Moreover, molecular dynamics simulations are also used to study the related mechanisms. It is found the added PS can lower the polymerization and crosslinking ratio during the curing process, in which alters the mechanical properties. Overall, these results indicate that *t*DPS is a promising material for the application of shape-memory polymer-based devices, and the corresponding computational works pave the way in front of understanding the mechanism and optimizing the design for SMP devices.

■ ASSOCIATED CONTENT

Supporting Information

The Supporting Information is available free of charge at https://pubs.acs.org/doi/10.1021/acsami.0c18413.

Differential scanning calorimetry (DSC) measurements, dynamic mechanical thermal analysis results (PDF)

Shape recovery of the *tDPS* sheet sample triggered by a hair dryer (MP4)

Shape recovery of the *tDPS* sheet sample triggered by hot water (MP4)

■ AUTHOR INFORMATION

Corresponding Author

Reza Mirzaeifar − *Department of Mechanical Engineering, Virginia Tech, Blacksburg, Virginia 24061, United States;* orcid.org/0000-0003-3427-0714; Phone: +1-540-231-8697; Email: rmirzaei@vt.edu; Fax: +1-540-231-2903; https://www.futurematerials-lab.com/

Authors

Kaiyuan Peng − *Department of Mechanical Engineering, Virginia Tech, Blacksburg, Virginia 24061, United States*

Yao Zhao − *Department of Mechanical Engineering, Virginia Tech, Blacksburg, Virginia 24061, United States*

Shima Shahab − *Department of Mechanical Engineering, Virginia Tech, Blacksburg, Virginia 24061, United States*

Complete contact information is available at: https://pubs.acs.org/10.1021/acsami.0c18413

Author Contributions

†K.P. and Y.Z. contributed equally to this work.

Notes

The authors declare no competing financial interest.

■ ACKNOWLEDGMENTS

Financial support from the NSF CMMI grant 2016474 is gratefully acknowledged.

■ REFERENCES

(1) Lendlein, A.; Kelch, S. Shape-Memory Polymers. *Angew. Chem., Int. Ed.* **2002**, *41*, 2034−2057.

(2) Liu, C.; Qin, H.; Mather, P. Review of Progress in Shape-Memory Polymers. *J. Mater. Chem.* **2007**, *17*, 1543−1558.

(3) Behl, M.; Razzaq, M. Y.; Lendlein, A. Multifunctional Shape-Memory Polymers. *Adv. Mater.* **2010**, *22*, 3388−3410.

(4) Menon, A. V.; Madras, G.; Bose, S. Shape Memory Polyurethane Nanocomposites with Porous Architectures for Enhanced Microwave Shielding. *Chem. Eng. J.* **2018**, *352*, 590−600.

(5) Fang, Z.; Zheng, N.; Zhao, Q.; Xie, T. Healable, Reconfigurable, Reprocessable Thermoset Shape Memory Polymer with Highly Tunable Topological Rearrangement Kinetics. *ACS Appl. Mater. Interfaces* **2017**, *9*, 22077−22082.

(6) Ze, Q.; Kuang, X.; Wu, S.; Wong, J.; Montgomery, S. M.; Zhang, R.; Kovitz, J. M.; Yang, F.; Qi, H. J.; Zhao, R. Magnetic Shape Memory Polymers with Integrated Multifunctional Shape Manipulation. *Adv. Mater.* **2020**, *32*, No. 1906657.

(7) Appiah, C.; Arndt, C.; Siemsen, K.; Heitmann, A.; Staubitz, A.; Selhuber-Unkel, C. Living Materials Herald a New Era in Soft Robotics. *Adv. Mater.* **2019**, *31*, No. 1807747.

(8) Xiao, R.; Huang, W. M. Heating/Solvent Responsive Shape-Memory Polymers for Implant Biomedical Devices in Minimally Invasive Surgery: Current Status and Challenge. *Macromol. Biosci.* **2020**, *20*, No. 2000108.

(9) Cichosz, S.; Masek, A.; Zaborski, M. Polymer-Based Sensors: A Review. *Polym. Test.* **2018**, *67*, 342−348.

(10) Gu, H.; Lee, S. W.; Buffington, S. L.; Henderson, J. H.; Ren, D. On-Demand Removal of Bacterial Biofilms Via Shape Memory Activation. *ACS Appl. Mater. Interfaces* **2016**, *8*, 21140−21144.

(11) Bhargava, A.; Peng, K.; Stieg, J.; Mirzaeifar, R.; Shahab, S. Focused Ultrasound Actuation of Shape Memory Polymers; Acoustic-Thermoelastic Modeling and Testing. *RSC Adv.* **2017**, *7*, 45452−45469.

(12) Melocchi, A.; Uboldi, M.; Inverardi, N.; Briatico-Vangosa, F.; Baldi, F.; Pandini, S.; Scalet, G.; Auricchio, F.; Cerea, M.; Foppoli, A.; et al. Expandable Drug Delivery System for Gastric Retention Based on Shape Memory Polymers: Development Via 4d Printing and Extrusion. *Int. J. Pharm.* **2019**, *571*, No. 118700.

(13) Sokolowski, W.; Metcalfe, A.; Hayashi, S.; Raymond, J.; et al. Medical Applications of Shape Memory Polymers. *Biomedical Materials* **2007**, *2*, S23−S27.

(14) Hardy, J. G.; Palma, M.; Wind, S. J.; Biggs, M. J. Responsive Biomaterials: Advances in Materials Based on Shape-Memory Polymers. *Adv. Mater.* **2016**, *28*, 5717−5724.

(15) Tong, Z.; Pei, X.; Shen, X.; Wei, S.; Gao, Y.; Huang, P.; Shi, B.; Sun, F.; Fu, T. An Enhanced Thermo-Actuated Shape Memory Polymer Composite Coupled with Elastomer. *Pet. Explor. Dev.* **2016**, *43*, 1097−1106.

(16) Gong, T.; Zhao, K.; Wang, W.; Chen, H.; Wang, L.; Zhou, S. Thermally Activated Reversible Shape Switch of Polymer Particles. *J. Mater. Chem. B* **2014**, *2*, 6855−6866.

(17) Zare, M.; Prabhakaran, M. P.; Parvin, N.; Ramakrishna, S. Thermally-Induced Two-Way Shape Memory Polymers: Mechanisms, Structures, and Applications. *Chem. Eng. J.* **2019**, *374*, 706−720.
(18) Huang, W. M.; Zhao, Y.; Wang, C. C.; Ding, Z.; Purnawali, H.; Tang, C.; Zhang, J. Thermo/Chemo-Responsive Shape Memory Effect in Polymers: A Sketch of Working Mechanisms, Fundamentals and Optimization. *J. Polym. Res.* **2012**, *19*, No. 9952.
(19) Lu, H.; Huang, W. M.; Fu, Y. Q.; Leng, J. Quantitative Separation of the Influence of Hydrogen Bonding of Ethanol/Water Mixture on the Shape Recovery Behavior of Polyurethane Shape Memory Polymer. *Smart Mater. Struct.* **2014**, *23*, No. 125041.
(20) Yang, J.; Wen, H.; Zhuo, H.; Chen, S.; Ban, J. A New Type of Photo-Thermo Staged-Responsive Shape-Memory Polyurethanes Network. *Polymers* **2017**, *9*, 287.
(21) Mirzaeifar, R.; DesRoches, R.; Yavari, A.; Gall, K. On Superelastic Bending of Shape Memory Alloy Beams. *Int. J. Solids Struct.* **2013**, *50*, 1664−1680.
(22) Mirzaeifar, R.; DesRoches, R.; Yavari, A. Analysis of the Rate-Dependent Coupled Thermo-Mechanical Response of Shape Memory Alloy Bars and Wires in Tension. *Continuum Mech. Thermodyn.* **2011**, *23*, 363−385.
(23) Wei, Z.; Sandstroröm, R.; Miyazaki, S. Shape-Memory Materials and Hybrid Composites for Smart Systems: Part I Shape-Memory Materials. *J. Mater. Sci.* **1998**, *33*, 3743−3762.
(24) Yakacki, C. M.; Shandas, R.; Lanning, C.; Rech, B.; Eckstein, A.; Gall, K. Unconstrained Recovery Characterization of Shape-Memory Polymer Networks for Cardiovascular Applications. *Biomaterials* **2007**, *28*, 2255−2263.
(25) Gall, K.; Yakacki, C. M.; Liu, Y.; Shandas, R.; Willett, N.; Anseth, K. S. Thermomechanics of the Shape Memory Effect in Polymers for Biomedical Applications. *J. Biomed. Mater. Res., Part A* **2005**, *73A*, 339−348.
(26) Lendlein, A.; Behl, M.; Hiebl, B.; Wischke, C. Shape-Memory Polymers as a Technology Platform for Biomedical Applications. *Expert Rev. Med. Devices* **2010**, *7*, 357−379.
(27) Wu, J.; Yuan, C.; Ding, Z.; Isakov, M.; Mao, Y.; Wang, T.; Dunn, M. L.; Qi, H. J. Multi-Shape Active Composites by 3d Printing of Digital Shape Memory Polymers. *Sci. Rep.* **2016**, *6*, No. 24224.
(28) Zarek, M.; Layani, M.; Cooperstein, I.; Sachyani, E.; Cohn, D.; Magdassi, S. 3d Printing of Shape Memory Polymers for Flexible Electronic Devices. *Adv. Mater.* **2016**, *28*, 4449−4454.
(29) Mao, Y.; Yu, K.; Isakov, M. S.; Wu, J.; Dunn, M. L.; Qi, H. J. Sequential Self-Folding Structures by 3d Printed Digital Shape Memory Polymers. *Sci. Rep.* **2015**, *5*, No. 13616.
(30) Choong, Y. Y. C.; Maleksaeedi, S.; Eng, H.; Wei, J.; Su, P.-C. 4d Printing of High Performance Shape Memory Polymer Using Stereolithography. *Mater. Des.* **2017**, *126*, 219−225.
(31) Wu, H.; Chen, P.; Yan, C.; Cai, C.; Shi, Y. Four-Dimensional Printing of a Novel Acrylate-Based Shape Memory Polymer Using Digital Light Processing. *Mater. Des.* **2019**, *171*, No. 107704.
(32) Antony, G. J. M.; Raja, S.; Aruna, S.; Jarali, C. S. Effect of the Addition of Diurethane Dimethacrylate on the Chemical and Mechanical Properties of Tba-Pegdma Acrylate Based Shape Memory Polymer Network. *J. Mech. Behav. Biomed. Mater.* **2020**, *110*, No. 103951.
(33) Bhargava, A.; Peng, K.; Mirzaeifar, R.; Shahab, S. In *Ultrasound Actuated Shape-Memory Polymer Based Drug Delivery Containers*, Active and Passive Smart Structures and IntegratedSystems XII; International Society for Optics and Photonics, 2018; 105952H.
(34) Bhargava, A.; Peng, K.; Shahab, S. In *Dynamics of Focused Ultrasound Actuated ShapeMemory Polymers*, Active and Passive Smart Structures and Integrated Systems XIII; International Society for Optics and Photonics, 2019; 1096720.
(35) Bhargava, A. Dynamics of Smart Materials in High Intensity Focused Ultrasound Field. Virginia Tech, 2020.
(36) Sun, L.; Huang, W.; Wang, C.; Zhao, Y.; Ding, Z.; Purnawali, H. Optimization of the Shape Memory Effect in Shape Memory Polymers. *J. Polym. Sci., Part A: Polym. Chem.* **2011**, *49*, 3574−3581.
(37) Sun, L.; Huang, W. M. Mechanisms of the Multi-Shape Memory Effect and Temperature Memory Effect in Shape Memory Polymers. *Soft Matter* **2010**, *6*, 4403−4406.
(38) Peng, K.; Shahab, S.; Mirzaeifar, R. Interaction of High-Intensity Focused Ultrasound with Polymers at the Atomistic Scale. *Nanotechnology* **2021**, *32*, No. 045707.
(39) Plimpton, S. Fast Parallel Algorithms for Short-Range Molecular Dynamics. *J. Comput. Phys.* **1995**, *117*, 1−19.
(40) Jewett, A. I.; Zhuang, Z.; Shea, J.-E. Moltemplate a Coarse-Grained Model Assembly Tool. *Biophys. J.* **2013**, *104*, 169a.
(41) Jewett, A. *Moltemplate Manual*; University of California: Santa Barbara, 2020. August 2015.
(42) Martínez, L.; Andrade, R.; Birgin, E. G.; Martínez, J. M. Packmol: A Package for Building Initial Configurations for Molecular Dynamics Simulations. *J. Comput. Chem.* **2009**, *30*, 2157−2164.
(43) Martínez, J. M.; Martínez, L. Packing Optimization for Automated Generation of Complex System's Initial Configurations for Molecular Dynamics and Docking. *J. Comput. Chem.* **2003**, *24*, 819−825.
(44) Stukowski, A. Visualization and Analysis of Atomistic Simulation Data with Ovito−the Open Visualization Tool. *Modell. Simul. Mater. Sci. Eng.* **2010**, *18*, No. 015012.
(45) Wu, X. L.; Huang, W. M.; Lu, H. B.; Wang, C. C.; Cui, H. P. Characterization of Polymeric Shape Memory Materials. *J. Polym. Eng.* **2017**, *37*, 1−20.
(46) Gooch, J. W. Tensile Hysteresis Curve. In *Encyclopedic Dictionary of Polymers*; Gooch, J. W., Ed.; Springer New York: New York, NY, 2011; pp 733.
(47) Beloshenko, V.; Beigel'zimer, Y. E.; Varyukhin, V.; Voznyak, Y. V. Strain hysteresis of polymers. *Dokl. Phys. Chem.* **2006**, *409*, 207−209.
(48) Dauber-Osguthorpe, P.; Roberts, V. A.; Osguthorpe, D. J.; Wolff, J.; Genest, M.; Hagler, A. T. Structure and Energetics of Ligand Binding to Proteins: *Escherichia Coli* Dihydrofolate Reductase-Trimethoprim, a Drug-Receptor System. *Proteins: Struct., Funct., Genet.* **1988**, *4*, 31−47.

https://dx.doi.org/10.1021/acsami.0c18413
ACS Appl. Mater. Interfaces XXXX, XXX, XXX−XXX